Sideroflexin 3 is an α-synuclein-dependent mitochondrial protein that regulates synaptic morphology

Inês S. Amorim[1,2], Laura C. Graham[2,3], Roderick N. Carter[4], Nicholas M. Morton[4], Fella Hammachi[5], Tilo Kunath[5], Giuseppa Pennetta[1,2], Sarah M. Carpanini[3], Jean C. Manson[3], Douglas J. Lamont[6], Thomas M. Wishart[2,3] and Thomas H. Gillingwater[1,2,*]

ABSTRACT

α-Synuclein plays a central role in Parkinson's disease, where it contributes to the vulnerability of synapses to degeneration. However, the downstream mechanisms through which α-synuclein controls synaptic stability and degeneration are not fully understood. Here, comparative proteomics on synapses isolated from α-synuclein^{−/−} mouse brain identified mitochondrial proteins as primary targets of α-synuclein, revealing 37 mitochondrial proteins not previously linked to α-synuclein or neurodegeneration pathways. Of these, sideroflexin 3 (SFXN3) was found to be a mitochondrial protein localized to the inner mitochondrial membrane. Loss of SFXN3 did not disturb mitochondrial electron transport chain function in mouse synapses, suggesting that its function in mitochondria is likely to be independent of canonical bioenergetic pathways. In contrast, experimental manipulation of SFXN3 levels disrupted synaptic morphology at the Drosophila neuromuscular junction. These results provide novel insights into α-synuclein-dependent pathways, highlighting an important influence on mitochondrial proteins at the synapse, including SFXN3. We also identify SFXN3 as a new mitochondrial protein capable of regulating synaptic morphology in vivo.

KEY WORDS: Alpha-synuclein, Sideroflexin 3, Neurodegeneration, Synapse, Mitochondria

INTRODUCTION

α-Synuclein is an abundant neuronal protein with a central role in the pathophysiology of Parkinson's disease. Abnormal accumulation of protein aggregates containing α-synuclein in Lewy bodies is a pathological hallmark of Parkinson's disease, and mutations and multiplications of *SNCA*, the gene encoding α-synuclein, have been linked with familial cases of the disease (Stefanis, 2012). The physiological and neurotoxic functions of

α-synuclein have been associated with a variety of cellular processes, including neurotransmission, protein degradation and mitochondrial function (Lashuel et al., 2013; Stefanis, 2012). For example, α-synuclein has previously been shown to affect mitochondrial functions including complex I activity, oxidative stress and protein import pathways (Di Maio et al., 2016; Liu et al., 2009; Parihar et al., 2008).

At the level of the synapse, α-synuclein supports neurotransmission by promoting SNARE complex assembly and regulating synaptic vesicle recycling and mobility (Burré et al., 2014; Murphy et al., 2000; Scott and Roy, 2012). However, whereas increased levels of α-synuclein attenuate the neurodegenerative phenotype caused by deletion of CSP-α (also known as DNAJC5) (Chandra et al., 2005), both increased expression and deletion of α-synuclein impair synaptic functions (Burre et al., 2010; Cabin et al., 2002; Nemani et al., 2010). Therefore, the molecular mechanisms through which α-synuclein influences synaptic form and function remain unclear.

Here, we have undertaken a proteomics screen to identify molecular pathways and proteins acting downstream of α-synuclein in synapses, identifying synaptic mitochondria and the mitochondrial protein SFXN3 as an important target.

RESULTS AND DISCUSSION

Identification of novel α-synuclein targets at the synapse

To uncover molecular mechanisms downstream of α-synuclein relevant for synaptic form and function, we quantified changes in the synaptic proteome of mice lacking α-synuclein (Fig. 1A). iTRAQ proteomics on synaptosomes from α-syn^{+/+} and α-syn^{−/−} mice identified 2615 individual proteins. Raw mass spectrometry data was filtered to leave only those proteins identified by at least two unique peptides and with expression levels consistently altered by ≥15% across two independent technical replicates (Table S1). The remaining 200 proteins were submitted to bioinformatics pathway analysis through ingenuity pathway analysis (IPA), DAVID and VarElect, revealing a striking enrichment of proteins (74 out of 200) belonging to mitochondrial pathways (Table 1; Table S1). This provides substantial experimental support for the hypothesis that α-synuclein has important physical and/or functional interactions with mitochondria (Haelterman et al., 2014; Nakamura, 2013). Further bioinformatics analysis identified 37 mitochondrial proteins not previously associated with α-synuclein or neurodegeneration (Fig. S1).

To select individual proteins from the shortlist of 37 to be prioritized for further analyses, we performed extensive literature searches to identify those with potential links to Parkinson's disease and/or neurodegeneration. Using this approach, sideroflexin 3 (SFXN3) was identified as a protein of particular interest. Studies have reported that levels of SFXN3 transcripts or protein were deregulated in the substantia nigra of Parkinson's disease patients and in rodents subjected to a 6-hydroxydopamine

[1]Centre for Integrative Physiology, University of Edinburgh, Hugh Robson Building, Edinburgh, EH8 9XD, UK. [2]Euan MacDonald Centre for Motor Neurone Disease Research, Chancellor's Building, University of Edinburgh, Edinburgh, EH16 4SB, UK. [3]Division of Neurobiology, The Roslin Institute and Royal (Dick) School of Veterinary Studies, University of Edinburgh, Edinburgh, EH25 9RG, UK. [4]Molecular Metabolism Group, University/BHF Centre for Cardiovascular Science, Queen's Medical Research Institute, University of Edinburgh, Edinburg, EH16 4TJ, UK. [5]MRC Centre for Regenerative Medicine, Institute for Stem Cell Research, The University of Edinburgh, Edinburgh, EH16 4UU, UK. [6]FingerPrints Proteomics Facility, College of Life Sciences, University of Dundee, Dundee, DD1 5EH, UK.

*Author for correspondence (T.Gillingwater@ed.ac.uk)

T.H.G., 0000-0002-0306-5577
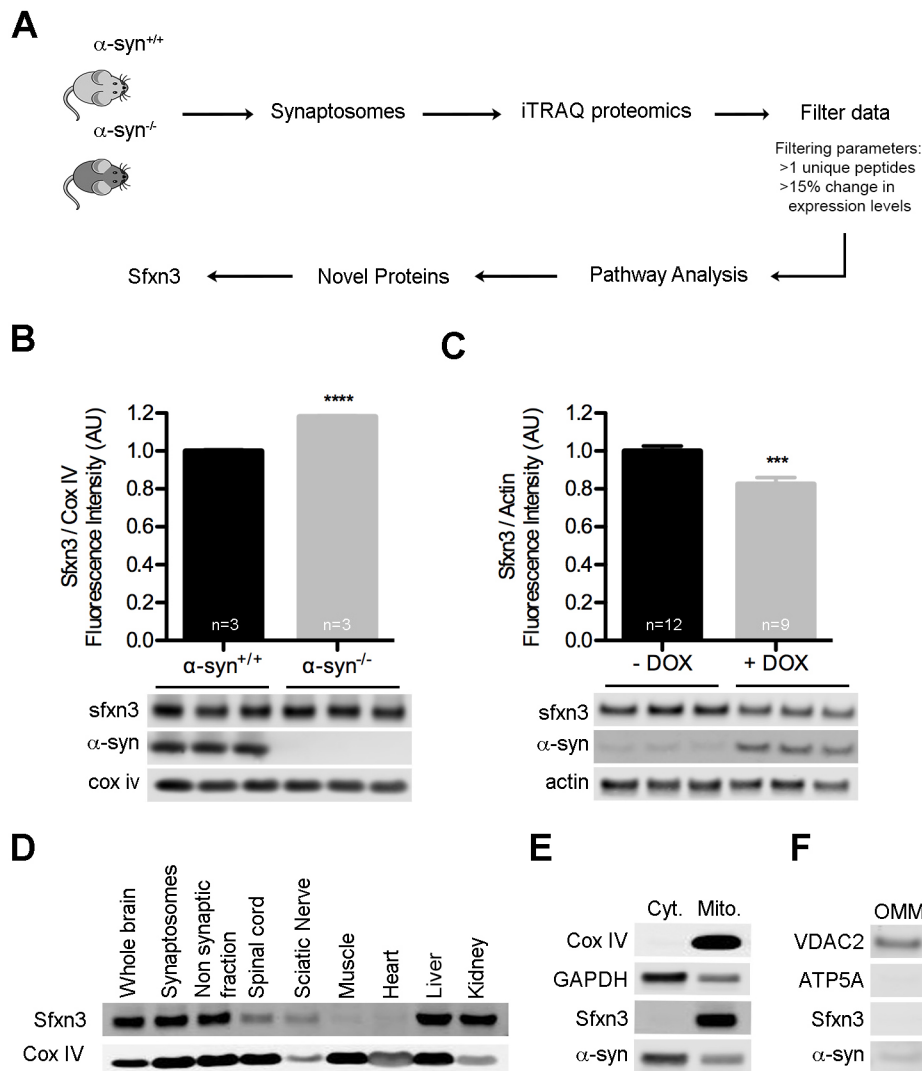
Fig. 1. Loss of α-synuclein at the synapse leads to widespread disruption of mitochondrial proteins, including SFXN3. (A) Schematic overview of experimental design. iTRAQ, isobaric tag for relative and absolute quantitation. (B) SFXN3 protein levels were significantly upregulated in synaptosomes from α-syn$^{-/-}$ compared to α-syn$^{+/+}$ controls. ****$P<0.0001$ (unpaired t-test). Cox IV, loading control. (C) SFXN3 protein levels were significantly reduced in SH-SY5Y cells overexpressing WT α-synuclein induced by doxycycline (+DOX). ***$P<0.001$ (unpaired t-test). Actin, loading control. (D) Representative western blot showing SFXN3 expression across several tissues from an adult wild-type mouse. Cox IV was used as a mitochondrial marker. (E) SFXN3 was exclusively localized to mitochondrial (Mito), but not cytosolic (Cyt), fractions isolated from mouse brain. Cox IV was used as a mitochondrial marker and GAPDH as a cytosolic marker. (F) SFXN3 was exclusively localized to the inner mitochondrial membrane. Outer mitochondrial membrane (OMM) and mitoplasts (Mit.) were isolated from undifferentiated SH-SY5Y cells. VDAC2 was used as a marker for the OMM and ATP5A as a marker for the mitoplast fraction. All data are mean±s.e.m.

lesion (Charbonnier-Beaupel et al., 2015; Fuller et al., 2014; Simunovic et al., 2009). SFXN1, a protein from the same family, interacts with connexin 32 (also known as GJB1), mutations in which cause Charcot–Marie–Tooth disease (Bergoffen et al., 1993; Fowler et al., 2013), and reduced levels of SFXN1 protein have been reported in Alzheimer's disease (Minjarez et al., 2016).

Table 1. Pathway and Gene Ontology analyses reveal an enrichment of mitochondrial proteins with modified levels in synapses lacking α-synuclein

	P-value
IPA top canonical pathways	
Mitochondrial dysfunction	9.36×10^{-8}
TCA cycle II (eukaryotic)	2.01×10^{-6}
Glutamate-dependent acid resistance	9.64×10^{-5}
Oxidative phosphorylation	1.15×10^{-5}
RhoA signalling	1.16×10^{-4}
DAVID GO annotation	
Generation of precursor metabolites and energy	2.30×10^{-9}
Transmission of nerve impulses	8.13×10^{-7}
Oxidative reduction	2.23×10^{-6}
Synaptic transmission	2.96×10^{-6}
Regulation of neurotransmitter levels	3.92×10^{-6}
Electron transport chain	2.46×10^{-5}

In addition, SFXN2 is upregulated in a dopaminergic cell line in response to rotenone treatment (Jin et al., 2007). SFXN3 belongs to a family of proteins (sideroflexins 1–5) that are putative iron transporters, with predicted transmembrane domains and mitochondrial localization (Fleming et al., 2001; Li et al., 2010). The functional role of these proteins, however, remains poorly understood.

Levels of SFXN3 protein were increased in synapses from α-syn$^{-/-}$ mice (Fig. 1B), suggesting that SFXN3 expression is inversely correlated with α-synuclein. To confirm this, we overexpressed wild-type α-synuclein in stably transfected SH-SY5Y cells. Exposure of SH-SY5Y cells to doxycycline (DOX) for 24 h led to a significant increase in α-synuclein (5.78±0.81; $n \geq 9$; mean±s.e.m.; $P=1.7 \times 10^{-6}$ in t-test), accompanied by a significant decrease in levels of SFXN3 protein (Fig. 1C). Thus, SFXN3 levels are bi-directionally regulated by α-synuclein.

It is not clear how α-synuclein regulates levels of SFXN3. One possibility is that α-synuclein interferes with the import of SFXN3 into mitochondria, given that α-synuclein has been shown to inhibit the import of nuclear-encoded mitochondrial proteins through an interaction with TOMM20 (Di Maio et al., 2016). In support of this, we found several mitochondrial import proteins, such as TIMM10B, PAM16 and TOMM40, to be upregulated in α-syn$^{-/-}$ mice compared to controls (Table S1).
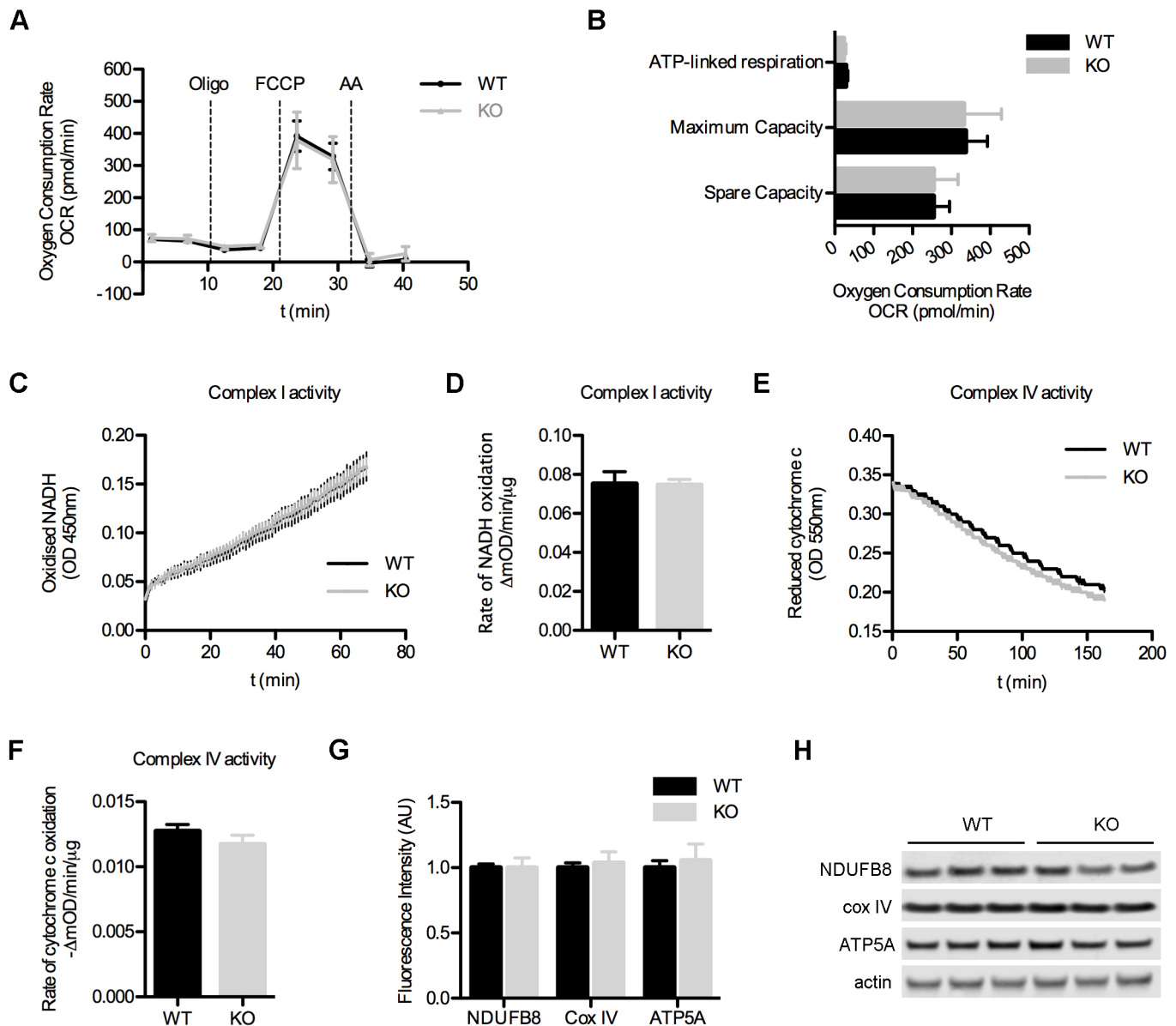
Fig. 2. Loss of SFXN3 does not affect mitochondrial bioenergetics. (A) Identical oxygen consumption rates (OCR) in synaptosomes from WT and SFXN3-KO mice. Dashed vertical lines indicate the time of injection of Oligomycin (Oligo), FCCP (FCCP) and antimycin A (AA). $n=3$. (B) Bioenergetic parameters derived from results in A (see Materials and Methods). $n=3$, $P>0.05$ (unpaired t-test). (C) Complex I activity measured by tracking absorbance of oxidized NADH. $n=3$. (D) Rate of Complex I activity derived from results in C shows that the enzymatic activity of Complex I is not compromised in SFXN3-KO mice. $n=3$, $P>0.05$ (unpaired t-test). (E) Complex IV activity measured by tracking absorbance of reduced cytochrome c. $n=3$. (F) Rate of Complex IV activity derived from results in E shows that the oxidation of cytochrome c is not affected in SFXN3-KO mice. $n=3$, $P>0.05$ (unpaired t-test). (G,H) Western blotting showing unaltered levels of key ETC proteins in synaptosomes from SFXN3-KO mice. $n=3$, $P>0.05$ (unpaired t-test). All data are mean±s.e.m.

SFXN3 is a mitochondrial protein enriched in the inner mitochondrial membrane

SFXN3 is predicted to be a mitochondrial protein (Pagliarini et al., 2008), but experimental evidence confirming its tissue expression and subcellular localization is lacking. We used western blotting to analyse expression levels of SFXN3 protein in mice (Fig. 1D). SFXN3 was highly enriched in brain, both in synaptic and non-synaptic fractions, spinal cord and peripheral nerve. It was also present in liver and kidney, but was not detectable in skeletal or cardiac muscle.

Isolation of mitochondrial and cytosolic fractions from mouse brain confirmed that SFXN3 was expressed exclusively in mitochondria (Fig. 1E). Furthermore, differential extraction of

mitochondrial outer membrane and mitoplasts of mitochondria from SH-SY5Y cells revealed that SFXN3 was localized to the mitoplast fraction (Fig. 1F). Given the presence of transmembrane domains in the SFXN3 protein (Li et al., 2010), we conclude that SFXN3 is preferentially localized to the inner mitochondrial membrane.

Loss of SFXN3 does not influence mitochondrial bioenergetics

The localization of SFXN3 to the inner mitochondrial membrane prompted us to ask whether SFXN3 plays a role in canonical bioenergetic pathways, including oxidative phosphorylation. We isolated purified synaptosomes from wild-type (WT) and SFXN3-knockout (KO) mice and performed mitochondrial respiration
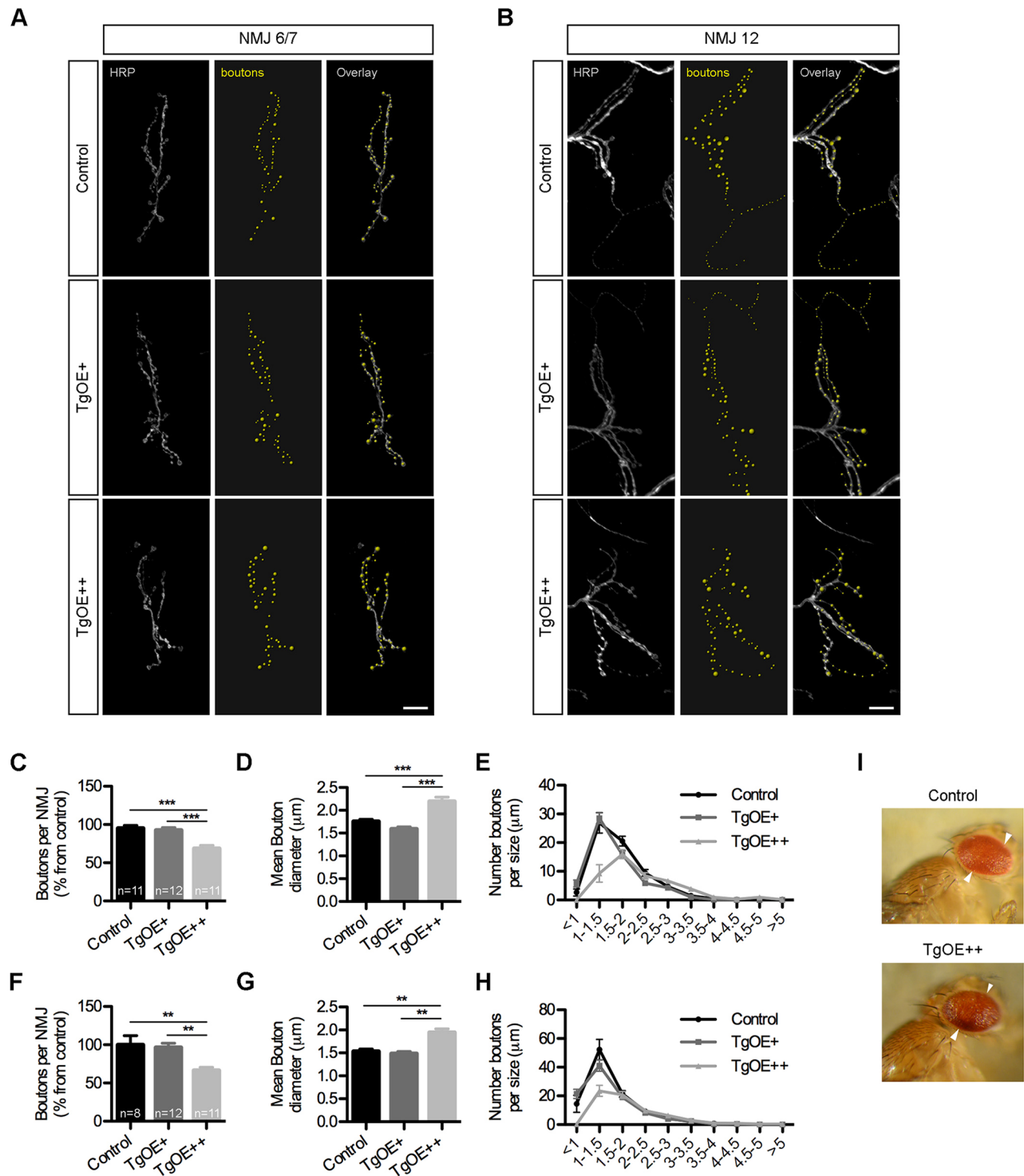
Fig. 3. Sfxn3 regulates synaptic morphology at the neuromuscular junction in *Drosophila*. (A,B) NMJs on muscles 6 and 7 (A) and 12 (B) of control and transgenic larvae, with low (TgOE+) and high (TgOE++) overexpression of SFXN3. Note the reduction in boutons in TgOE++ NMJs (grey, anti-HRP; yellow, pseudo-coloured synaptic boutons). Scale bars: 10 µm. (C–H) Reduction in the number of boutons and increase in mean bouton diameter on NMJs from muscles 6 and 7 (C,D) and 12 (F,G) overexpressing SFXN3 (TgOE++). Results are mean±s.e.m. **P<0.01, ***P<0.001 (one-way ANOVA with Tukey post-test). Distribution of bouton diameter from NMJs on muscles 6 and 7 (E) and 12 (H) showing a specific reduction of small size (<1.5 µm) boutons in TgOE++ larvae. (I) Representative images of eyes from control and TgOE++ flies demonstrating no overt phenotype.

assays using a Seahorse XF^{e}24 Analyzer. Oxygen consumption rates (OCR) during basal respiration were similar between WT and SFXN3-KO mice (Fig. 2A). Accordingly, the fraction of ATP-linked respiration was comparable in WT and SFXN3-KO mice

(Fig. 2B). Uncoupling of mitochondria, by using FCCP, induced equivalent spare and maximum respiratory OCR rates in WT and SFXN3-KO synaptosomes, indicating that synaptic mitochondria from SFXN3-KO mice are comparable to those from controls with

respect to their ability to cope with short periods of high energetic demand (Fig. 2A,B). Thus, SFXN3 is not absolutely required for mitochondrial bioenergetics pathways, as mitochondrial respiration was unaffected by the absence of SFXN3.

To confirm that subtle effects on mitochondrial respiration prompted by reduced levels of SFXN3 were not being masked by compensatory mechanisms in enzymatic activity or abundance of other key electron transport chain (ETC) proteins, we performed enzymatic assays on immunocaptured Complex I and Complex IV (Fig. 2C,E). The rates of NADH and cytochrome *c* oxidation revealed identical enzymatic activities of Complex I and Complex IV, respectively, in WT and SFXN3-KO mice (Fig. 2D,F). Quantitative western blotting for ATP5A (a component of ATP synthase), and the Complex I and IV proteins NDUFB8 and Cox IV confirmed that no compensatory changes were occurring in these ETC proteins in SFXN3-KO mice (Fig. 2G,H).

SFXN3 influences synaptic morphology at the *Drosophila* neuromuscular junction

Given that SFXN3 was identified as a α-synuclein target in synaptic mitochondria, we wanted to establish whether SFXN3 contributes to pathways regulating synaptic stability. We obtained and mapped a UAS-driven P{EPgy2} *Drosophila* strain demonstrating insertion of the promoter in the correct direction and in the 5′UTR of our gene of interest, suggesting significant potential for overexpression of SFXN3 (*Drosophila* homologue of the sideroflexin gene; FlyBase annotation CG6812). The *Drosophila* UAS-Gal4 system was used to generate tissue-specific overexpression of SFXN3 in third-instar larval neurons using the pan-neuronal driver *elav-Gal4*. High-dose overexpression of SFXN3 (TgOE++) led to a significant reduction in the number of synaptic boutons, accompanied by an overall increase in mean bouton diameter, at the neuromuscular junctions (NMJs) from muscles 6 and 7 and from muscle 12 (Fig. 3). The most striking phenotype was a reduction in type II boutons innervating muscle 12. To confirm that these changes were occurring as a direct result of changes in SFXN3 levels, we repeated our analyses with a low dose overexpression of SFXN3 (TgOE+). These experiments confirmed no alterations in any of the neuromuscular parameters analysed (Fig. 3). Furthermore, analysis of eye morphology in TgOE++ flies showed no overt phenotype (Fig. 3I). The *Drosophila* eye is a robust and sensitive read-out for identifying neurodegeneration (Sanhueza et al., 2015), suggesting that overexpression of SFXN3 selectively influences synaptic morphology without initiating neurodegenerative cascades.

Taken together, our results demonstrate an important role for α-synuclein in regulating mitochondrial proteins at the synapse. We identify SFXN3 as one mitochondrial protein whose levels are bi-directionally regulated by α-synuclein and that is also capable of directly influencing synapses *in vivo*. Further studies will now be required to determine the extent to which SFXN3 acts as a key intermediary of α-synuclein-dependent synaptic pathology occurring in Parkinson's disease. Considering that α-synuclein itself is difficult to target from a therapeutic perspective (as a result of being intrinsically disordered, with diverse and poorly understood oligomeric states), targeting SFXN3 might ultimately represent an alternative strategy for maintaining synapses in Parkinson's disease.

MATERIALS AND METHODS
Reagents
All chemicals were purchased from Sigma Aldrich, except tissue culture reagents, the BCA assay, RIPA buffer and Halt protease inhibitor cocktail, which were from Thermo Scientific, and Percoll, which was from GE Healthcare Biosciences. Buffer compositions are in Table S2.

Mice
C57Bl/6J (α-syn$^{+/+}$) and C57Bl/6JOlaHsd (α-syn$^{-/-}$) mice, carrying a natural α-synuclein deletion (Specht and Schoepfer, 2001), were obtained from University of Edinburgh breeding stocks. Sfxn3$^{tm1b(KOMP)Wtsi}$ mice (SFXN3-KO mice; http://www.mousephenotype.org/data/genes/MGI:2137679) were obtained from the Wellcome Trust Sanger Institute Mouse Genetics Project as part of the nPad MRC Mouse Consortium, maintained on a C57Bl/6N background. Mice were of mixed gender and 2–4 months old. All work was covered by appropriate UK Home Office licenses.

Drosophila
Drosophila melanogaster were raised on standard cornmeal food at room temperature. *elav-Gal4* and *GMR-Gal4* driver strains were used with stocks obtained from the Bloomington *Drosophila* stock center (IDs: y^1 w^{67c23}; P{EPgy2}CG6812^{EY02703}; Canton-S). Crosses were maintained at 22°C for 24 h before removal of adults and embryos were incubated in a water bath to increase levels and activity of Gal4 proteins. Incubation temperatures were 25°C and 30°C for low dose (TgOE+) or high dose (TgOE++) overexpression experiments, respectively. For immunohistochemistry methods see Sanhueza et al. (2015). Images were analysed using IMARIS software to determine the number and transverse diameter of synaptic boutons. The investigator was blinded to the group allocation throughout.

Isolation of synaptosomes and iTRAQ proteomics analysis
Isolation of crude synaptosomes from α-syn$^{+/+}$ and α-syn$^{-/-}$ mice was performed as described previously (McGorum et al., 2015; Wishart et al., 2012). Samples were homogenized in iTRAQ buffer and supernatant extracts from four mice per genotype were pooled. 100 µg protein was labelled with tags (114 and 116 α-syn$^{+/+}$; 115 and 117 α-syn$^{-/-}$) before injection into an Ultimate RSLC nano UHPLC system coupled to a LTQ Orbitrap Velos Pro (Thermo Scientific). Results were filtered to include proteins identified by at least two unique peptides with a ≥15% difference in levels across both α-syn$^{+/+}$ vs α-syn$^{-/-}$ comparisons.

Data were examined using bioinformatics tools: ingenuity pathway analysis (IPA; Ingenuity Systems, USA); Database for Annotation, Visualization and Integrated Discovery (DAVID; NIH, USA); and VarElect (LifeMap Sciences, USA). IPA was used to determine affected molecular pathways (Top Canonical Pathways). DAVID Functional Annotation was used to identify enrichment for gene ontology (GO) terms. VarElect was used to identify the fraction of data that included proteins associated with the terms 'mitochondria' and the group of terms 'Parkinson's', 'Parkinson', 'PD', 'synuclein' and 'SNCA'.

Tissue culture
SH-SY5Y cells were electroporated with a Tet-One™ plasmid (Clontech) encoding full-length human α-synuclein and a DOX-responsive clonal line was selected and maintained in Dulbecco's modified Eagle's medium (DMEM) supplemented with 10% fetal bovine serum (FBS), 1% penicillin-streptomycin, 1 mM sodium pyruvate and 2 µg/ml puromycin. For induction of α-synuclein expression, 24 h after plating cells were differentiated for 5 days in the presence of 10 µM retinoic acid and incubated in DMEM supplemented with 10 µg/ml of doxycycline for 24 h.

Isolation and fractionation of mitochondria
Mitochondria were isolated from mouse brain using the Mitochondria Isolation Kit for Tissue (Abcam). Fractionation of mitochondria from undifferentiated SH-SY5Y cells was performed as described previously (Nishimura et al., 2014).

Western blotting
Western blotting was performed as described previously (Eaton et al., 2013), using antibodies in Table S3.

Mitochondrial respiration assays
Mitochondrial respiration assays were performed on purified synaptosomes, isolated from mouse forebrain using discontinuous Percoll gradients prepared in isolation medium, as previously described (Choi et al., 2009).

Synaptosomes (10 µg protein/well, ≥5 technical replicas per sample) were loaded into wells of XF^{e}24 V7 (Seahorse Biosciences) uncoated plates. The plate was centrifuged at 2000 *g* for 20 min at 4°C, and 500 µl of incubation medium was added to each well prior to entry into the XF^{e}24 Seahorse Analyzer (Seahorse Biosciences). Oxygen consumption rates (OCR) were measured in groups of two cycles of 1 min wait, 1 min mix, 3 min measurements, with an injection between each 2 cycles. Each well was sequentially exposed to 4 µg/ml oligomycin to stop ATPsynthase activity, 4 µM FCCP to dissipate mitochondrial membrane potential and potentiate maximum oxidative phosphorylation activity, and 4 µg/ml antimycin A to inhibit complex IV and completely stop mitochondria oxidative phosphorylation. OCR values for each injection step were calculated as the mean of the measurements of two cycles per injection step and used to determine the following parameters: basal respiration (basal mitochondrial respiration before addition of any compound); ATP-linked respiration (basal minus oligomycin-induced rate, respiration rates associated with the production of ATP by the ATP synthase); maximum capacity (FCCP-induced minus antimycin-A-induced rate, maximum respiratory capacity achieved by the activity of complex I–IV); and spare capacity (FCCP-induced minus basal rate, mitochondria capacity above basal levels that can be recruited in situations of high energetic demand).

Enzymatic assays

Enzymatic assays were performed using the Complex I and IV Enzyme Activity Microplate Assay kits (Abcam) according to the manufacturer's instructions.

Statistical analysis

Quantitative data was collected using Microsoft Excel. Statistics for pathway analysis and gene ontology enrichments were calculated by their respective software, using the right-tailed Fisher's exact test. All other statistics were performed using GraphPad Prism® (detailed in the results section or figure legends). Statistical significance was considered to be $P<0.05$.

References

Bergoffen, J., Scherer, S. S., Wang, S., Scott, M. O., Bone, L. J., Paul, D. L., Chen, K., Lensch, M. W., Chance, P. F. and Fischbeck, K. H. (1993). Connexin mutations in X-linked Charcot-Marie-Tooth disease. *Science* **262**, 2039-2042.

Burre, J., Sharma, M., Tsetsenis, T., Buchman, V., Etherton, M. R. and Sudhof, T. C. (2010). Alpha-synuclein promotes SNARE-complex assembly in vivo and in vitro. *Science* **329**, 1663-1667.

Burré, J., Sharma, M. and Südhof, T. C. (2014). alpha-Synuclein assembles into higher-order multimers upon membrane binding to promote SNARE complex formation. *Proc. Natl. Acad. Sci. USA* **111**, E4274-E4283.

Cabin, D. E., Shimazu, K., Murphy, D., Cole, N. B., Gottschalk, W., McIlwain, K. L., Orrison, B., Chen, A., Ellis, C. E., Paylor, R. et al. (2002). Synaptic vesicle depletion correlates with attenuated synaptic responses to prolonged repetitive stimulation in mice lacking alpha-synuclein. *J. Neurosci.* **22**, 8797-8807.

Chandra, S., Gallardo, G., Fernández-Chacón, R., Schlüter, O. M. and Südhof, T. C. (2005). Alpha-synuclein cooperates with CSPalpha in preventing neurodegeneration. *Cell* **123**, 383-396.

Charbonnier-Beaupel, F., Malerbi, M., Alcacer, C., Tahiri, K., Carpentier, W., Wang, C., During, M., Xu, D., Worley, P. F., Girault, J.-A. et al. (2015). Gene expression analyses identify Narp contribution in the development of L-DOPA-induced dyskinesia. *J. Neurosci.* **35**, 96-111.

Choi, S. W., Gerencser, A. A. and Nicholls, D. G. (2009). Bioenergetic analysis of isolated cerebrocortical nerve terminals on a microgram scale: spare respiratory capacity and stochastic mitochondrial failure. *J. Neurochem.* **109**, 1179-1191.

Di Maio, R., Barrett, P. J., Hoffman, E. K., Barrett, C. W., Zharikov, A., Borah, A., Hu, X., McCoy, J., Chu, C. T., Burton, E. A. et al. (2016). alpha-Synuclein binds to TOM20 and inhibits mitochondrial protein import in Parkinson's disease. *Sci. Transl. Med.* **8**, 342ra78.

Eaton, S. L., Roche, S. L., Llavero Hurtado, M., Oldknow, K. J., Farquharson, C., Gillingwater, T. H. and Wishart, T. M. (2013). Total protein analysis as a reliable loading control for quantitative fluorescent western blotting. *PLoS ONE* **8**, e72457.

Fleming, M. D., Campagna, D. R., Haslett, J. N., Trenor, C. C., III and Andrews, N. C. (2001). A mutation in a mitochondrial transmembrane protein is responsible for the pleiotropic hematological and skeletal phenotype of flexed-tail (f/f) mice. *Genes Dev.* **15**, 652-657.

Fowler, S. L., Akins, M., Zhou, H., Figeys, D. and Bennett, S. A. L. (2013). The liver connexin32 interactome is a novel plasma membrane-mitochondrial signaling nexus. *J. Proteome Res.* **12**, 2597-2610.

Fuller, H. R., Hurtado, M. L., Wishart, T. M. and Gates, M. A. (2014). The rat striatum responds to nigro-striatal degeneration via the increased expression of proteins associated with growth and regeneration of neuronal circuitry. *Proteome Sci.* **12**, 20.

Haelterman, N. A., Yoon, W. H., Sandoval, H., Jaiswal, M., Shulman, J. M. and Bellen, H. J. (2014). A mitocentric view of Parkinson's disease. *Annu. Rev. Neurosci.* **37**, 137-159.

Jin, J., Davis, J., Zhu, D., Kashima, D. T., Leroueil, M., Pan, C., Montine, K. S. and Zhang, J. (2007). Identification of novel proteins affected by rotenone in mitochondria of dopaminergic cells. *BMC Neurosci.* **8**, 67.

Lashuel, H. A., Overk, C. R., Oueslati, A. and Masliah, E. (2013). The many faces of alpha-synuclein: from structure and toxicity to therapeutic target. *Nat. Rev. Neurosci.* **14**, 38-48.

Li, X., Han, D., Kin Ting Kam, R., Guo, X., Chen, M., Yang, Y., Zhao, H. and Chen, Y. (2010). Developmental expression of sideroflexin family genes in Xenopus embryos. *Dev. Dyn.* **239**, 2742-2747.

Liu, G., Zhang, C., Yin, J., Li, X., Cheng, F., Li, Y., Yang, H., Uéda, K., Chan, P. and Yu, S. (2009). alpha-Synuclein is differentially expressed in mitochondria from different rat brain regions and dose-dependently down-regulates complex I activity. *Neurosci. Lett.* **454**, 187-192.

McGorum, B. C., Pirie, R. S., Eaton, S. L., Keen, J. A., Cumyn, E. M., Arnott, D. M., Chen, W., Lamont, D. J., Graham, L. C., Llavero Hurtado, M. et al. (2015). Proteomic profiling of cranial (Superior) cervical ganglia reveals beta-amyloid and ubiquitin proteasome system perturbations in an equine multiple system neuropathy. *Mol. Cell. Proteomics* **14**, 3072-3086.

Minjarez, B., Calderón-González, K. G., Rustarazo, M. L. V., Herrera-Aguirre, M. E., Labra-Barrios, M. L., Rincon-Limas, D. E., Del Pino, M. M. S., Mena, R. and Luna-Arias, J. P. (2016). Identification of proteins that are differentially expressed in brains with Alzheimer's disease using iTRAQ labeling and tandem mass spectrometry. *J. Proteomics* **139**, 103-121.

Murphy, D. D., Rueter, S. M., Trojanowski, J. Q. and Lee, V. M. (2000). Synucleins are developmentally expressed, and alpha-synuclein regulates the size of the presynaptic vesicular pool in primary hippocampal neurons. *J. Neurosci.* **20**, 3214-3220.

Nakamura, K. (2013). alpha-Synuclein and mitochondria: partners in crime? *Neurotherapeutics* **10**, 391-399.

Nemani, V. M., Lu, W., Berge, V., Nakamura, K., Onoa, B., Lee, M. K., Chaudhry, F. A., Nicoll, R. A. and Edwards, R. H. (2010). Increased expression of alpha-synuclein reduces neurotransmitter release by inhibiting synaptic vesicle reclustering after endocytosis. *Neuron* **65**, 66-79.

Nishimura, N., Gotoh, T., Oike, Y. and Yano, M. (2014). TMEM65 is a mitochondrial inner-membrane protein. *PeerJ* **2**, e349.

Pagliarini, D. J., Calvo, S. E., Chang, B., Sheth, S. A., Vafai, S. B., Ong, S.-E., Walford, G. A., Sugiana, C., Boneh, A., Chen, W. K. et al. (2008). A mitochondrial protein compendium elucidates complex I disease biology. *Cell* **134**, 112-123.

Parihar, M. S., Parihar, A., Fujita, M., Hashimoto, M. and Ghafourifar, P. (2008). Mitochondrial association of alpha-synuclein causes oxidative stress. *Cell. Mol. Life Sci.* **65**, 1272-1284.

Sanhueza, M., Chai, A., Smith, C., McCray, B. A., Simpson, T. I., Taylor, J. P. and Pennetta, G. (2015). Network analyses reveal novel aspects of ALS pathogenesis. *PLoS Genet.* **11**, e1005107.

Scott, D. and Roy, S. (2012). alpha-Synuclein inhibits intersynaptic vesicle mobility and maintains recycling-pool homeostasis. *J. Neurosci.* **32**, 10129-10135.

Simunovic, F., Yi, M., Wang, Y., Macey, L., Brown, L. T., Krichevsky, A. M., Andersen, S. L., Stephens, R. M., Benes, F. M. and Sonntag, K. C. (2009). Gene expression profiling of substantia nigra dopamine neurons: further insights into Parkinson's disease pathology. *Brain* **132**, 1795-1809.

Specht, C. G. and Schoepfer, R. (2001). Deletion of the alpha-synuclein locus in a subpopulation of C57BL/6J inbred mice. *BMC Neurosci.* **2**, 11.

Stefanis, L. (2012). α-synuclein in Parkinson's disease. *Cold Spring Harb. Perspect. Med.* **2**, a009399.

Wishart, T. M., Rooney, T. M., Lamont, D. J., Wright, A. K., Morton, A. J., Jackson, M., Freeman, M. R. and Gillingwater, T. H. (2012). Combining comparative proteomics and molecular genetics uncovers regulators of synaptic and axonal stability and degeneration in vivo. *PLoS Genet.* **8**, e1002936.

Supplementary Information for Amorim et al.

Table S1. Proteomics filtered data-set.

UniProt	Description	Ratio	Mitochondria Evidence	Novel
Q9DB15	39S ribosomal protein L12, mitochondrial	1.17	Y	Y
P63038	60 kDa heat shock protein, mitochondrial	1.16	Y	N
Q3TQP7	Acetyl-CoA Acetyltransferase 1	1.17	Y	Y
Q14BV7	Acyl-Coenzyme A binding domain containing 6	0.74	N	N / A
Q546G4	Albumin 1 (Precursor)	1.17	Y	N
Q9CZS1	Aldehyde dehydrogenase X, mitochondrial	1.22	Y	Y
Q3UJW9	Aldo-Keto Reductase Family 1, Member A1 (Aldehyde Reductase)	1.16	Y	N
B2RUJ5	Amyloid beta A4 precursor protein-binding family A member 1	0.74	N	N / A
B1AV14	Apolipoprotein, MICOS complex subunit Mic27	1.16	Y	Y
Q53YU5	Apoptosis repressor interacting with CARD	0.83	Y	Y
Q5SUV9	Aromatic-L-amino-acid decarboxylase (Fragment)	1.26	N	N / A
Q3TGE1	ARP3 Actin-Related Protein 3 Homolog	0.71	N	N / A
Q9DB20	ATP synthase subunit	1.32	Y	N
Q06185	ATP synthase subunit e, mitochondrial	0.73	Y	Y
Q8CF81	ATP-dependent Clp protease proteolytic subunit	1.19	Y	Y
A2AUK5	Band 4.1-like protein 1	0.78	N	N / A
A2AHX9	Bcl-2-like protein 1 (Fragment)	0.63	Y	N
Q91ZZ3	Beta-synuclein	1.44	Y	N
Q3U6G1	Biliverdin reductase B (Flavin reductase (NADPH))	1.18	N	N / A
P61022	Calcineurin B homologous protein 1	0.76	N	N / A
P62204	Calmodulin	0.74	N	N / A
G3UXG7	Casein kinase II subunit beta	1.23	N	N / A
Q9JM96	Cdc42 effector protein 4	1.18	N	N / A
B1AUQ7	Centrin-2 (Fragment)	0.69	N	N / A
Q9CQ10	Charged multivesicular body protein 3	0.73	N	N / A
Q9D8B3	Charged multivesicular body protein 4b	0.77	N	N / A
Q3TJ95	Clathrin, Light Chain B	1.25	N	N / A
Q921J6	Cldn10 protein (Fragment)	0.82	N	N / A
O89079	Coatomer subunit epsilon	0.77	N	N / A
Q544Y7	Cofilin 1, non-muscle	1.16	Y	N
Q3UHW9	Cofilin 2	1.22	N	N / A
Q5SNY8	Coiled-coil domain-containing protein 104 (Fragment)	0.77	N	N / A
Q3UHB8	Coiled-coil domain-containing protein 177	0.83	N	N / A
Q52L78	Cryab protein	1.39	Y	N
P19536	Cytochrome c oxidase subunit 5B, mitochondrial	1.37	Y	N
O88485	Cytoplasmic dynein 1 intermediate chain 1	0.80	N	N / A
O35459	Delta(3,5)-Delta(2,4)-dienoyl-CoA isomerase, mitochondrial	1.19	Y	N
E9Q557	Desmoplakin	1.36	N	N / A
A8QKB4	Destrin (Fragment)	1.26	N	N / A
Q8CDG3	Deubiquitinating protein VCIP135	0.84	N	N / A
A2ALF0	DnaJ homolog subfamily C member 8	0.72	N	N / A
Q3TPZ5	Dynactin 2	0.77	Y	N
Q9Z0Y1	Dynactin subunit 3	1.16	N	N / A
Q3TBU6	Dynamin 2	1.22	N	N / A
P62878	E3 ubiquitin-protein ligase RBX1	0.79	N	N / A
Q99KR6	E3 ubiquitin-protein ligase RNF34	0.81	N	N / A
Q9EQG7	Ectonucleotide pyrophosphatase/phosphodiesterase family member 5	0.76	N	N / A
Q2YDW1	Eif3j protein (Fragment)	0.79	N	N / A
Q99LC5	Electron transfer flavoprotein subunit alpha, mitochondrial	1.23	Y	Y
A2AWI7	Endophilin-B2	1.28	N	N / A
Q3URM4	Endoplasmic Reticulum Protein 44	0.79	N	N / A
P57759	Endoplasmic reticulum resident protein 29	0.79	N	N / A
Q8BH95	Enoyl-CoA hydratase, mitochondrial	1.21	Y	Y
Q5EBJ4	Ermin	1.21	N	N / A
Q9D172	ES1 protein homolog, mitochondrial	1.29	N	N / A
CK054	Ester hydrolase C11orf54 homolog	1.27	N	N / A

G3UX44	Estradiol 17-beta-dehydrogenase 8 (Fragment)	1.19	N	N / A
Q3TDD8	Eukaryotic Translation Initiation Factor 4B	0.79	N	N / A
P63242	Eukaryotic translation initiation factor 5A-1	0.65	Y	Y
Q9CRS5	EWS RNA-Binding Protein 1	0.78	N	N / A
Q5EBJ0	Fatty acid binding protein 3, muscle and heart	1.47	N	N / A
Q497I3	Fatty acid binding protein 5, epidermal	1.46	N	N / A
P51880	Fatty acid-binding protein, brain	1.27	N	N / A
P26049	Gamma-aminobutyric acid receptor subunit alpha-3	0.77	N	N / A
Q8C3E3	GDP-D-Glucose Phosphorylase 1	0.80	N	N / A
A7VJ98	Glia maturation factor beta	0.65	N	N / A
P03995	Glial fibrillary acidic protein	0.79	Y	N
Q548L6	Glutamate decarboxylase	1.17	Y	N
Q548L4	Glutamate decarboxylase	1.18	N	N / A
F6VNW5	Glutamate--cysteine ligase regulatory subunit (Fragment)	0.75	N	N / A
Q8VD04	GRIP1-associated protein 1	0.82	N	N / A
Q99LP6	GrpE protein homolog 1, mitochondrial	1.23	Y	Y
A2ARF6	GTP:AMP phosphotransferase AK4, mitochondrial (Fragment)	1.27	Y	N
Q3U931	GTPase Activating Protein (SH3 Domain) Binding Protein 2	0.83	N	N / A
Q3UKC8	Guanine nucleotide-binding protein subunit gamma	1.19	N	N / A
Q9R257	Heme-binding protein 1	1.50	N	N / A
Q3TGN5	Heterogeneous Nuclear Ribonucleoprotein U (Scaffold Attachment Factor A)	0.83	N	N / A
P70349	Histidine triad nucleotide-binding protein 1	1.42	N	N / A
A0JLV3	Histone H2B (Fragment)	1.41	N	N / A
E0CZ27	Histone H3 (Fragment)	1.27	N	N / A
Q6B822	Histone H4 (Fragment)	1.37	N	N / A
Q9Z2Y3	Homer protein homolog 1	0.80	N	N / A
Q61249	Immunoglobulin-binding protein 1	0.67	N	N / A
Q9D7P6	Iron-sulfur cluster assembly enzyme ISCU, mitochondrial	1.32	Y	Y
D3YTT4	Isobutyryl-CoA dehydrogenase, mitochondrial	1.21	Y	Y
Q9D6R2	Isocitrate dehydrogenase [NAD] subunit alpha, mitochondrial	1.17	Y	Y
Q684I8	Isocitrate dehydrogenase 3 (NAD+), gamma (Fragment)	1.23	Y	Y
Q3TY86	Isoform 2 of Apoptosis-inducing factor 3	0.80	Y	N
Q9D164	Isoform 2 of FXYD domain-containing ion transport regulator 6	0.83	N	N / A
Q68FH0	Isoform 2 of Plakophilin-4 n	1.24	N	N / A
Q62442	Isoform 2 of Vesicle-associated membrane protein 1	1.23	Y	N
Q8R0S4	Isoform 2 of Voltage-dependent L-type calcium channel subunit beta-4	0.84	N	N / A
O88935	Isoform 3 of Synapsin-1	1.20	N	N / A
P09470	Isoform Testis-specific of Angiotensin-converting enzyme	0.77	Y	N
Q9JHI5	Isovaleryl-CoA dehydrogenase, mitochondrial	1.27	Y	Y
Q3TTY6	Lin-7 Homolog C	1.34	N	N / A
B5TVM9	Lisch-like isoform 7	0.81	N	N / A
P70699	Lysosomal alpha-glucosidase	1.19	Y	N
P08249	Malate dehydrogenase, mitochondrial	1.24	Y	Y
Q545I9	MC3T3-E1 calcyclin	1.19	N	N / A
Q5I0U7	MCG122050	1.19	N	N / A
B2RX66	MCG124812	0.77	N	N / A
Q5SQB7	MCG68069	0.77	N	N / A
G3X997	Metallo-beta-lactamase domain-containing protein 2	0.72	N	N / A
Q9EQ20	Methylmalonate-semialdehyde dehydrogenase [acylating], mitochondrial	1.25	Y	Y
P10637	Microtubule-associated protein tau	0.68	Y	N
Q91VR7	Microtubule-associated proteins 1A/1B light chain 3A	1.22	Y	N
G8DXN9	Mitochondrial ATP synthase epsilon subunit (Fragment)	1.30	Y	N
D3YVK5	Mitochondrial import inner membrane translocase subunit Tim10 B	1.35	Y	Y
Q9CQV1	Mitochondrial import inner membrane translocase subunit TIM16	1.30	Y	Y
Q9QYA2	Mitochondrial import receptor subunit T	1.16	Y	N
Q8VEA4	Mitochondrial intermembrane space import and assembly protein 40	1.36	Y	Y
D3YWY6	Mitochondrial pyruvate carrier 1	1.16	Y	Y
Q9JMF0	mRNA, clone:2-63 (Fragment)	0.72	N	N / A
Q3THE2	Myosin regulatory light chain 12B	0.77	N	N / A
Q8K4Z3	NAD(P)H-hydrate epimerase	1.20	Y	Y
Q99LC3	NADH dehydrogenase [ubiquinone] 1 alpha subcomplex subunit 10, mitochondrial	1.27	Y	N

Q9CQ91	NADH dehydrogenase [ubiquinone] 1 alpha subcomplex subunit 3	1.25	Y	N
Q9CQZ5	NADH dehydrogenase [ubiquinone] 1 alpha subcomplex subunit 6	1.29	Y	N
O09111	NADH dehydrogenase [ubiquinone] 1 beta subcomplex subunit 11, mitochondrial	0.55	Y	N
Q9CQC7	NADH dehydrogenase [ubiquinone] 1 beta subcomplex subunit 4	1.20	Y	N
Q6R891	Neurabin-2	0.77	N	N / A
P06837	Neuromodulin	0.78	N	N / A
Q3U3C2	Niemann-Pick Disease, Type C2	1.16	N	N / A
Q3TV28	Nucleobindin 2	0.74	N	N / A
Q5NC81	Nucleoside diphosphate kinase	1.18	Y	Y
Q9CTE1	Nucleosome Assembly Protein 1-Like 5	1.16	N	N / A
Q8BFY6	Peflin	0.81	N	N / A
Q3TE63	Peptidyl-prolyl cis-trans isomerase	1.43	Y	N
Q99KR7	Peptidyl-prolyl cis-trans isomerase F, mitochondrial	1.33	Y	N
Q3UWS9	Peroxiredoxin 5	1.99	Y	N
B1AXW5	Peroxiredoxin-1 (Fragment)	1.21	Y	N
Q9JJV2	Profilin-2	1.39	N	N / A
Q9DB60	Prostamide/prostaglandin F synthase	1.19	N	N / A
Q5D098	Proteasome subunit beta type (Fragment)	0.82	N	N / A
D6RI64	Protein 1110004F10Rik	0.78	N	N / A
Q9DCM0	Protein ETHE1, mitochondrial	1.23	Y	N
Q8BHZ0	Protein FAM49A	0.75	N	N / A
Q8BUK6	Protein Hook homolog 3	0.84	N	N / A
Q8JZS0	Protein lin-7 homolog A	1.19	N	N / A
Q9D0R8	Protein LSM12 homolog	1.17	N	N / A
H3BKQ7	Protein Ppp1r9a	0.81	N	N / A
Q3UFJ3	Pyruvate dehydrogenase E1 alpha 1	1.21	Y	Y
P34022	Ran-specific GTPase-activating protein	0.78	N	N / A
Q05186	Reticulocalbin-1	1.18	N	N / A
Q5FWK3	Rho GTPase-activating protein 1	1.26	N	N / A
P70122	Ribosome maturation protein SBDS	0.81	N	N / A
Q3URG1	RIKEN cDNA 2900041A09, isoform CRA_a	1.17	Y	N
Q545E6	RNA-binding protein	0.74	N	N / A
G3UXT7	RNA-binding protein FUS (Fragment)	0.80	N	N / A
H3BJI4	RWD domain containing 4A, isoform CRA_b	0.68	N	N / A
Q9JL08	S100 calcium binding protein A1 (Fragment)	0.70	Y	Y
Q545H7	S100 calcium binding protein A13	1.32	N	N / A
Q3ULN6	Saccharopine Dehydrogenase (Putative)	1.16	Y	Y
Q3TT51	Secretogranin V, isoform CRA_b	0.82	N	N / A
D3YWV5	Semaphorin-4A	0.82	N	N / A
B2RUC7	Serine/threonine kinase receptor associated protein	0.81	N	N / A
Q3UEI6	SERPINE1 MRNA Binding Protein 1	0.77	N	N / A
Q3U4F0	Sideroflexin-3	1.16	Y	Y
Q8BJI1	Sodium-dependent neutral amino acid transporter SLC6A17	0.73	N	N / A
Q61609	Sodium-dependent phosphate transporter 1	0.74	N	N / A
Q80UP8	Sodium-dependent phosphate transporter 2	0.69	N	N / A
Q80U52	Sodium/hydrogen exchanger (Fragment)	0.78	Y	Y
D3YYN7	Sodium/potassium-transporting ATPase subunit alpha-2	0.83	N	N / A
Q3UYK6	Solute carrier family 1 (Glial high affinity glutamate transporter), member 2	0.80	N	N / A
Q3US35	Solute Carrier Family 1 (Glutamate/Neutral Amino Acid Transporter), Member 4	0.77	N	N / A
Q67BT3	Solute carrier family 13 member 5	0.74	N	N / A
Q8BPS5	Solute Carrier Family 16 (Monocarboxylate Transporter), Member 1	0.77	Y	Y
P17809	Solute carrier family 2, facilitated glucose transporter member 1	0.53	Y	Y
Q9CX10	Solute Carrier Family 25, Member 27	1.24	Y	Y
Q14C53	Solute carrier family 39 (Zinc transporter), member 7	0.63	N	N / A
Q62417	Sorbin and SH3 domain-containing protein 1	0.81	N	N / A
D3Z789	Sorting nexin-3	1.31	N	N / A
Q9Z2I9	Succinyl-CoA ligase [ADP-forming] subunit beta, mitochondrial	1.21	Y	Y
Q9WUM5	Succinyl-CoA ligase [ADP/GDP-forming] subunit alpha, mitochondrial	1.18	Y	Y
Q3UK61	Succinyl-CoA:3-ketoacid-coenzyme A transferase	1.22	Y	Y
Q3U8W4	Superoxide dismutase	1.22	Y	N
P08228	Superoxide dismutase [Cu-Zn]	1.28	Y	N

Q64332	Synapsin-2	1.23	N	N / A
Q9ERB0	Synaptosomal-associated protein 29	0.76	N	N / A
I3PMU3	Syndecan (Fragment)	0.57	N	N / A
P70452	Syntaxin-4	0.78	N	N / A
Q3UKC1	Tax1-binding protein 1 homolog	0.76	N	N / A
P97930	Thymidylate kinase	1.16	Y	Y
A2AEC2	Transcription elongation factor A protein-like 3 (Fragment)	0.75	N	N / A
P62869	Transcription elongation factor B polypeptide 2	1.23	N	N / A
Q8VDE3	Translation elongation factor (Fragment)	1.17	Y	Y
Q8CHW4	Translation initiation factor eIF-2B subunit epsilon	0.76	N	N / A
P63028	Translationally-controlled tumor protein	0.80	Y	N
Q9JKK7	Tropomodulin-2	0.72	N	N / A
O54818	Tumor protein D53	1.18	N	N / A
P24529	Tyrosine 3-monooxygenase	1.16	Y	N
Q3T992	Ubiquilin 1	1.25	N	N / A
A2RTT4	Ubiquitin-Conjugating Enzyme E2N	1.29	N	N / A
O08759	Ubiquitin-protein ligase E3A	0.80	N	N / A
F2Z452	Uncharacterized protein	0.75	N	N / A
Q8VE95	UPF0598 protein C8orf82 homolog	1.40	N	N / A
Q99KC8	von Willebrand factor A domain-containing protein 5A	0.77	N	N / A
E0CYH4	WD repeat-containing protein 26	0.82	N	N / A
D3Z7N4	Zinc transporter ZIP6 (Fragment)	0.65	N	N / A

UniProt: Uniprot Accession; Description: Protein description; Ratio: Ratio between the expression levels of a given protein in α-syn-/- mice compared to α-syn+/+. Average of two technical replicas; Mitochondria Evidence: N: No. Y: Yes. Evidence that a given protein is localised in mitochondria; or that it influences or is influenced by mitochondrial function; Novel N: No; Y: Yes; N/A: Not Applicable. Evidence that a given protein has previously been associated with α-synuclein, Parkinson's Disease or Neurodegeneration in general.

## Table S2: Buffer compositions.

Buffer	Compound	Concentration
iTRAQ buffer	Urea	6 M
	Thio-urea	2M
	CHAPS	2%
	SDS	0.5%
	Protease Inhibitors	1%
Isolation Media pH 7.4	Sucrose	225 mM
	Mannitol	75 mM
	EGTA	1 mM
	HEPES	5 mM
Incubation Media 37°C	NaCl	120 mM
	KCl	3.5 mM
	CaCl2	1.3 mM
	KH2PO4	0.4 mM
	Na2SO4	1.2 mM
	MgSO4	2 mM
	Glucose	15 mM
	Pyruvate	10 mM
	Fatty-acid free BSA	4 mg/mL

Table S3: Antibodies used for Western Blotting.

Antibody	Catalog No	Supplier	Concentration
α-synuclein	sc-7011-R	santa cruz biotechnology	1:5000
β-actin	ab8226	abcam	1:5000
ATP5A	ab176569	abcam	1:5000
COX IV	ab14744	abcam	1:1000
GAPDH	ab9484	abcam	1:1000
NDUFB8	MS105	Mitosciences	1:1000
sfxn3	HPA008028	Sigma Aldrich	1:400
VDAC 2	ab47104	abcam	1:500
IRDye® 800CW Donkey anti-Mouse IgG (H + L)	926-32212	LiCOR Biosciences	1:5000
IRDye® 680RD Donkey anti-Rabbit IgG (H + L)	926-68073	LiCOR Biosciences	1:5000

For use with anti-α-synuclein antibodies, the membranes were fixed in 0.4% PFA in PBS for 20 min and washed in PBS prior to blocking, as this method has been shown to increase the sensitivity of α-synuclein detection (Lee and Kamitani, 2011).
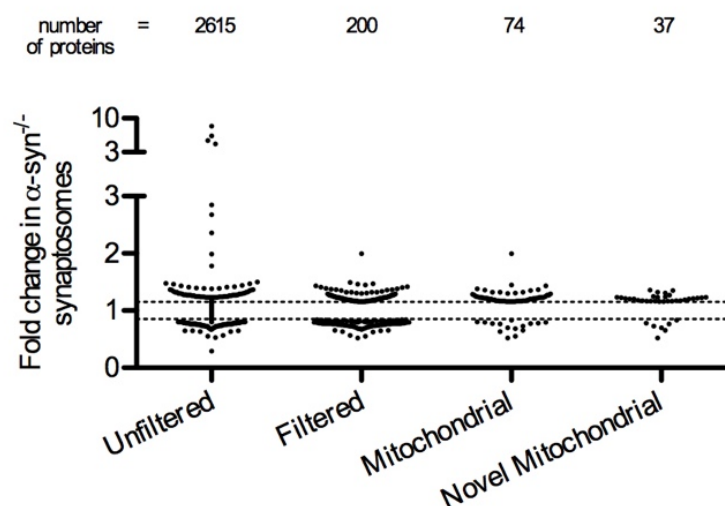
Figure S1: Graphical representation of the filtering steps taken during the analysis of iTRAQ proteomics data. Y-axis represents the mean fold change, from two technical replicates, of each protein in α-syn^{-/-} synaptosomes when compared to control α-syn^{+/+} synaptosomes. "Unfiltered" column includes all 2,615 proteins identified by iTRAQ. "Filtered" column contains the subset of identified protein which met the selection criteria of being identified by more than 1 unique peptide and being altered by more than 15% in two technical replicates. Since mitochondrial pathways were shown to be some of the most affected in α-syn^{-/-} mice (Table 1), the 200 filtered proteins were further selected to include only mitochondrial proteins ("Mitochondrial" column, 74 proteins). Mitochondrial proteins were further filtered to include proteins not previously associated with α-synuclein or neurodegeneration (see methods). These group of 37 proteins, here referred to as "novel

mitochondrial", was prioritized for a literature search on subtle links to synaptic stability and neurodegenerative processes.

References

Lee, B. R. and Kamitani, T. (2011). Improved immunodetection of endogenous alpha-synuclein. *PLoS One* **6**, e23939.